IOP Conf. Series: Materials Science and Engineering **418** (2018) 012097 doi:10.1088/1757-899X/418/1/012097

Phenomenological friction model in deep drawing of aluminum sheet metals

Daniel Wiklund[1], Mats Larsson[2]

[1]Swerea IVF, Box 104, SE-431 22 Mölndal, Sweden
[2]University West, Department of Production Processes, SE-461 86 Trollhättan, Sweden

daniel.wiklund@swerea.se

Abstract. Friction is an important parameter in sheet metal forming since it influences the flow of material in the process. Consequently, it is also an important parameter in the design process of new stamping dies when numerical simulations are utilized. Today, the most commonly used friction model in forming simulations is Coulomb´s friction which is a strong simplification of the tribological system conditions and a contributory cause of discrepancy between simulation and physical experiments. There are micromechanical models available but with an inherent complexity that results in limited transparency for users. The objective in this study was to design a phenomenological friction model with a natural level of complexity when Coulomb´s friction is inadequate. The local friction model considers implicit properties of tool and sheet surface topography, lubricant viscosity, sheet metal hardness and strain, and process parameters such as sliding speed and contact pressure. The model was calibrated in a Bending-Under-Tension test (BUT) and the performance was evaluated in a cross shaped geometry (X-die). The results show a significant improvement of the simulation precision and provide the user a transparent tribological system.

1. Introduction

The sheet metal forming operation is influenced by several process parameters and material properties. The research on material models has significantly improved the precision of numerical sheet metal forming processes during the years. However, friction is also an important parameter since it influences the flow of material in forming operations and indirectly the stress and strain distribution, spring back phenomena, risk of failure etc. Today, Coulomb´s friction is the most commonly used model for numerical simulations in the design process of stamping tools. But Coulomb´s friction is not sufficient to describe the tribological conditions and is therefore a contributory cause of discrepancy between simulation and physical experiments.

Therefore, several attempts have been made to develop models for large-scale forming simulations which consider local micro-scale effects of friction, from simple, e.g. [1-4], to more advanced models, e.g. [5-9]. The drawback with the simple models is that they consider too limited influencing parameters or only are valid in restrictive conditions and therefore seldom are useful the design process of stamping tools. In recent years, advanced models have been fully developed and are now available [8-9]. This is a promising step towards more viable tribological engineering tools. However, the highly specialized models require stand-alone software or tabulated data from such to be utilized. Consequently, a major leap has to be taken if the Coulomb´s friction is inadequate for a specific application. The purpose of

this study is to bridge this gap by a complementary, transparent model. An efficiently model is needed which can be calibrated with limited investment and efforts. In this study a fundamental friction model [7] is further developed and evaluated.

2. Experimental work

Two physical experimental tests were performed. Bending-Under-Tension tests were performed to map the frictional response of the system and then a deep-drawing operation was used to study the influence of friction.

2.1. The Tribotest

The friction tests were performed in a Bending-Under-Tension friction rig, see Figure 1. The test simulates the die radius conditions in a stamping tool. A steel sheet strip is bent and drawn over a cylindrical tool bar under tension. The lubricant was hot-melt drylube Anticorit PL 39 SX from Fuchs with the amount of 1.0±0.2 g/m2. The tool material was a nodular iron (GGG70L) with a hard chromium coating, Sa-roughness of 0.23±0.04 µm (Robust Gaussian Filter, 0.25mm). In continuous production the tool temperature is elevated and therefore the tool pin was heated to 50 degrees Celsius to simulate production conditions.

2.2. The Cross Die test

A verifying test was performed in a hydraulic press, a deep drawing operation with a cross shaped geometry (X-die), see figure 2. The lubricant amount was 0.8±0.1 g/m2. The tool material was Sleipner and the die was coated by Wolfram Carbide.

2.3. The sheet material

The sheet material was Aluminum AA6016, thickness 1.0 mm.

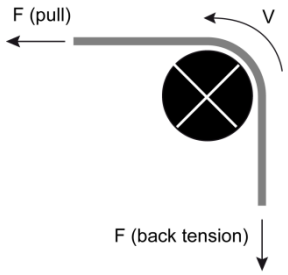

Figure 1. Schematic representation of the Bending-Under-Tension friction test.

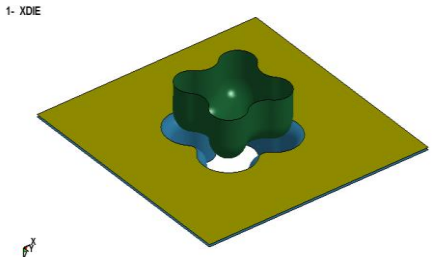

Figure 2. Cross Die test - (green), Die (blue) and Blankholder (yellow).

3. Friction model

Firstly we express the normal and tangential load balances.

$$pA = p_c A_c + p_h(A - A_c) \quad (1)$$

$$\mu pA = \tau_c A_c + \tau_h(A - A_c) \quad (2)$$

where the local nominal mean pressure p is partly shared by the real mean asperity contact pressure p_c and the lubricant hydrodynamic mean pressure p_h, and A is the local nominal area and A_c the real contact area. The local coefficient of friction is represented by μ,τ_c is the real contact mean shear stress and τ_h is the hydrodynamic mean shear stress.

Secondly, we make the same hydrodynamic definitions and assumptions as Löfgren [10] in Eq. 3-10. Define the Hersey parameters and the hydrodynamic coefficient of friction as

$$He = \frac{\eta V}{p} \tag{3}$$

$$He_{\mathrm{h}} = \frac{\eta V}{p_{\mathrm{h}}} \tag{4}$$

$$\mu_{\mathrm{h}} = \frac{\tau_{\mathrm{h}}}{p_{\mathrm{h}}} \tag{5}$$

where η is the dynamic viscosity and V the sliding velocity.

Besides the Newton´s law of viscosity Eq. (6), we assume, in accordance with Emmens [11], that the behavior of the hydrodynamic coefficient of friction is proportional to the square root of He_h in all hydrodynamic regimes.

Thirdly, we define the Hersey parameters and the hydrodynamic coefficient of friction as

$$\tau_{\mathrm{h}} = \frac{\eta V}{s} \tag{6}$$

$$\mu_{\mathrm{h}} \propto \sqrt{He_{\mathrm{h}}} \tag{7}$$

Consequently

$$\frac{He_{\mathrm{h}}}{s^2} = \frac{\mu_{\mathrm{h}}}{s} = c \tag{8}$$

$$\frac{p_{\mathrm{h}}}{p} = \frac{He}{He_0}\left(\frac{\sigma}{s}\right)^2 \tag{9}$$

$$\frac{\tau_{\mathrm{h}}}{p} = \mu_0 \frac{He}{He_0}\frac{\sigma}{s} \tag{10}$$

where c is the Emmens constant, s represents separation and σ is the surface standard deviation. Emmens showed that $He_0=c(Rpm)^2$ where Rpm is the average height of the five highest roughness peaks measured from the centre line [11]. However, if a Gaussian distribution is assumed, then the standard deviation could be used instead, consequently we here assume $He_0=c\sigma^2$.

In the next step the classical theories on plastic contact of rough surfaces are introduced. In experiments, Pullen [12] indented a rough soft surface with a hard flat one. By flattening the rough surface a height distance (h), Pullen observed flattening of the highest asperities, but also a general rise (u) of the surface from its original position. The separation between the surfaces, defined as the distance between their mean planes, could then be expressed as s=h+u.

Introducing a surface height distribution ϕ(z), the degree of contact may be written as

$$\alpha = \int_h^\infty \phi(z)dz, \tag{11}$$

and the unit rise and separation as

$$u = \int_h^\infty (z-h)\phi(z)dz, \tag{12}$$

$$s = h + \int_h^\infty (z-h)\phi(z)dz. \tag{13}$$

Assume a Gaussian distribution but utilize the following approximation to avoid the inconvenience with infinite tails [13]

$$\phi(\delta) = \frac{35}{96}\left[1-\left(\frac{\delta}{3\sigma}\right)^2\right]^3 \tag{14}$$

where δ is a surface height and ($-3 \leq \delta/\sigma \leq 3$).

This means the real contact area ratio can be expressed as

$$\alpha = (-1+h^*)^4(1+4h^*+10h^{*2}+20h^{*3}), \tag{15}$$

and the dimensionless separation (s*) as

$$s^* = -h^{*5}(5h^{*3} - 20h^{*2} + 28h^* - 14), \tag{16}$$

where h*=h/σ. Note that the integral domain is altered in the final step, i.e. (0≤h*≤1) in Equation 15 and 16!

Based on the observation of Pullen the Effective Hardness (p_c/H) can be expressed as

$$\frac{p_c}{H} = \frac{1}{(1-\alpha)} \tag{17}$$

In order to improve the accuracy of the contact growth, the model is extended with some degrees of freedom. Firstly, the consequence of Eq. 17 means that the Effective Hardness approaches infinity in fully developed contact. An infinite persistence is not a realistic physical assumption and therefore it is limited by introducing an Ultimate Persistence Coefficient (UPC), (q), see Eq. 18. This implies if q=0, then p_c=H, and the material exerts no persistence (just hardness), and if q=1 the persistence is represented according to Pullen. Secondly, it is noticed that Eq. 18, which is shown in the original paper, poorly represents the experimental results at low contact ratios (α<0.3), see Figure 3. A Contact-Hardening Coefficient (CHC), (n), is therefore introduced, see Eq. 19. Finally, in order to control the contact growth, a dimensionless Contact-Hardening Ratio (CHR), (H_r) is introduced. This parameter controls the tilting effect of the curve, see Fig 3.

$$\frac{p_c}{H} = \frac{H_r}{(1-q\alpha^n)} \tag{18}$$

where

$$n = 1 - (atan(c_1 + c_2 \propto) + c_3)/c_4 \tag{19}$$

Additionally, it has been shown that the effective hardness is influenced by bulk plastic strain. Analytical expressions have been derived for plane stress and strain [14, 15]. Simple strain dependence can be expressed by adding plastic strain, (ε_P), to Eq. 19. Calibrating the Strain Dependence (SD), (w), and the Strain Coefficient (SC), (m), strong correlations (R^2>0.9, (0.05< ε_P<1)) can be obtained between analytical expressions and Eq. 20.

$$\frac{p_c}{H} = \frac{H_r}{(1-q\alpha^n+w\varepsilon_p^m)} \tag{20}$$

Finally, the dimensionless normal load balance Eq. 1 can be expressed by using Eq. 9,

$$\frac{p_c}{p}\alpha + \frac{He}{He_0}\left(\frac{\sigma}{s}\right)^2(1-\alpha) - 1 = 0, \tag{21}$$

and friction coefficient by using Eq. 2, and 10,

$$\mu = \frac{\mu_c p_c \alpha}{p} + \frac{\mu_0 He}{He_0}\frac{\sigma}{s}(1-\alpha), \tag{22}$$

and assuming a proportional contact shear stress to contact pressure, i.e. $\tau_c=\mu_c P_c$ where μ_c is the real contact coefficient of friction. The second term in Eq. 22 represents the influence of lubricant shear stress. The term has limited significance in sheet metal forming and consequently discarded in this study. Also, pure hydrodynamic lubrication is assumed to have limited significance and consequently μ=0 when He/He_0>1.

3.1. Shear stresses

The real contact coefficient of friction μ_c is influenced by the tool surface roughness. Challen and Oxley have modeled ploughing and adhesion of wedge-shaped asperity deformation [16]. When a rigid asperity indents a soft flat surface, friction becomes a function of the effective attack angle. However, in fully

plastic contacts individual summits join together to form contact patches [17]. According to Ma, the tool surface is intersected at a specific height and each contact patch is then fitted by a paraboloid. The intersected area of a patch is equated by the area of the ellipse and the height can be determined by equating the volume of the patch. However, in the LS-Dyna subroutine directionally dependent friction cannot be considered. Consequently, a spherical segment is utilized in this work instead of a paraboloid. The attack angle becomes the ratio between height and radius of a spherical segment:

$$\frac{h}{r} = \frac{2V_m}{A_m^{3/2}\sqrt{2/\pi}} \tag{23}$$

where Vm and Am are the measured volume and the intersected area of a specific patch [18]. The attack angle of an intersected height is calculated as a weighted average of patches, see Figure 4. The attack angle, θ, is represented by

$$\theta = a_1(a_2 + \alpha)^{a_3}, \tag{24}$$

where a_1, a_2, a_3, are three constants.

The results from the study of Challen and Oxley can be simplified when the angles are low, which applies for tool surfaces. Friction can then be modeled by an adhesive component, μ_a plus the influence from the attack angle, μ_θ, see Eq. 26. The influence from the attack angle is represented by Eq. 24, however the order of contribution from the attack angle needs to be adjusted by fitting the parameter a_1 which will scale Eq. 24.

Hydrodynamic effects are apparent already at low speeds. It is assumed that these effects are generated by constrictions, probably in nanoscale, that occur in the contact zone. These complex hydrodynamic phenomena generate extremely fine lubricating films that reduce shear stress in the contact zone. In the absence of a good model the phenomena is roughly modeled by Emmen´s formulation, i.e. 1-He/He_0 [10]. However, since the hydrodynamic effects occur in the contact zone the apparent pressure is replaced by contact pressure p_c.

$$\mu_\delta = \Delta\mu\left(1 - \frac{\eta V}{p_c He_c}\right), \tag{25}$$

where Δμ is the additional low speed contribution and He_c relates to constrictions in the contact zone.

$$\mu_c = \mu_a + \mu_\theta + \mu_\delta \tag{26}$$

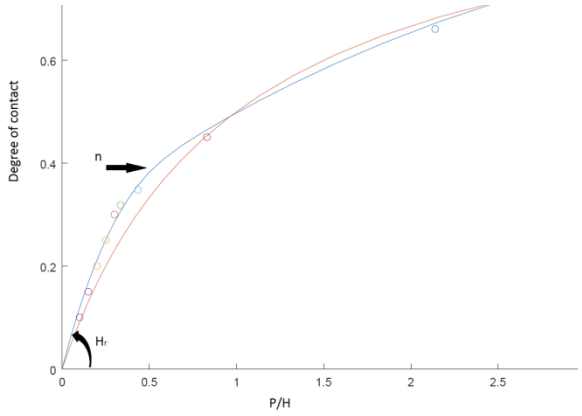

Figure 3. Dimensionless load vs. Degree of contact. Encircled markings are read out from Pullens experiments. Modified n and Hr parameters improves the precision.

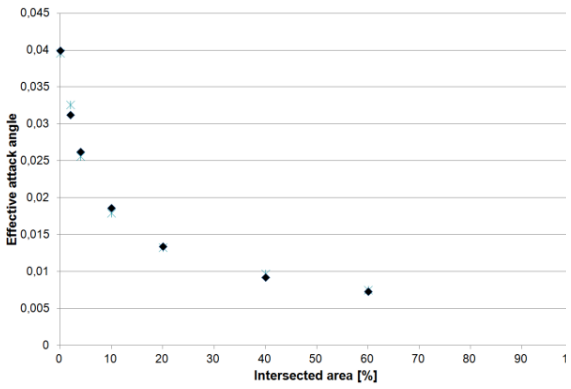

Figure 4. Weighted effective attack angle vs. intersected areas.

4. Numerical methods

The numerical simulations were carried out with the finite element program LS-Dyna and LS-Opt [18-19]. BARLAT_YLD2000 was the utilized material model. Hardening was represented by load curves in three directions.

4.1. Calculation scheme

The following calculation scheme has been used, i) initial/new guess of compression, ii) calculation of contact area and separation, Eq.15-16, iii) evaluate normal load balance, Eq. 19-21, iv) iteration i-iii until tolerance acceptable, v) calculate contact friction Eq. 24-25, vi) calculate friction, Eq. 22.

5. Results

5.1. The tribotests

The frictional response of the BUT-test was measured with different sliding speeds with two different radiuses, see figure 5. The frictional response drops rapidly between 1 to 27 mm/s and at higher speeds there is a more moderate decrease. At the speed of 10 mm/s there is also one measurement result for radius 6 mm. This shows a rapid drop of the frictional response from radius 10 to radius 6, and then a very small decrease between 6 to 3.6 mm, see figure 5.

5.2. Calibration of friction model

With a limited amount of data, only a rough calibration could be performed. Firstly, the contact stiffness was calibrated utilizing the obtained results for 10 mm/s, i.e. three radiuses and an extrapolated value for zero pressure. The CHC, derived from the paper of Pullen was used as a starting value. Then Hardness and CHR could be calculated. The results did show that the CHC, had to be adjusted, i.e. a stronger curvature was necessary. The UPC was set equal to one, and the fitted data to the analytical expression was utilized for SD and SC.

Secondly, a linear regression of the four measurement values at 60 and 100 mm/s was calculated. Based on the regression the Hersey parameter (He_0) could be estimated. The regression line intersects 0 mm/s at friction 0.117. Friction parameter, a1, is adjusted to this level, i.e. results obtained with a large radius (low pressure) will be slightly higher than 0.117 and results obtained with a small radius (high pressures) will be slightly lower than 0.117.

Finally, regression is calculated based on 6 measured values at 1-27 mm/s, and He_c is calculated.

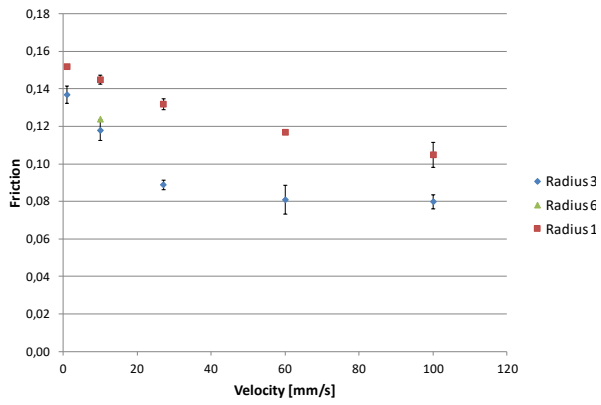

Figure 5. Sliding speed vs. obtained friction in the BUT-test.

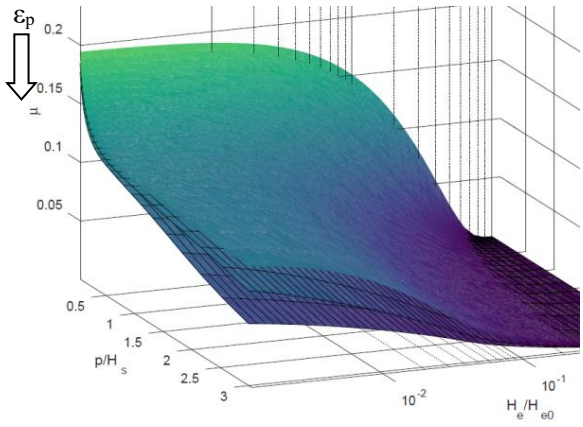

Figure 6. The dimensionless load and Hersey parameter vs. friction. Increased plastic strains reduce friction and a knee is formed for saturated contact. Low speed effects are not shown.

5.3. Verifying Cross Die tests

In physical experiments the sheet material was drawn until fracture. Numerically the maximum drawing depth was predicted by the forming limit diagram. The results are presented in Table 1.

Table 1. Results of X-die. The table shows the maximum depth before fracture in physical experiments and in numerical simulations with variable and static friction, respectively. The tests were performed at two different drawing speeds.

Velocity (mms^{-1})	Experimental results	Variable friction	Static friction (μ=0.15)
5	39.7	40.5	41.1
45	43.5	43.8	41.1

6. Discussion

The purpose of this work was to develop a phenomenological friction model with a natural level of complexity when Coulomb´s friction is inadequate. The model was based on the observations made by Emmens concerning hydrodynamic effects, by Pullen concerning contact persistence and separation, and by Oxley and Ma concerning plowing effects. Besides, some additional degrees of freedom were added in order to create a better phenomenological description, as well. By this approach a transparent model was developed. Thereby, the basic physics and formulations are available for a user.

In its simplest, the model demands in total 7 parameters to describe the frictional behavior, hardness, viscosity, Emmens Hersey parameter, and four parameters related to the contact friction. The effective hardness is described by Pullens formulation (1/1-α), and thereby no extra parameters are needed.

In a more advanced version, strain dependence could be added which means 2 extra parameters. Moreover, if the effective hardness should be modeled in detail there are additionally 2 to 6 parameters needed, this despite the fact that the model does not express all effects explicitly, for example, both resistance and material hardening are lumped together. Finally, to model hydrodynamic phenomena that occurs in low speed demands at least 2 extra parameters. Consequently, there is a rapid increase in complexity if the system should be modeled in detail.

In the experimental work, the polishing direction was applied perpendicular to the sliding direction. This is the normal procedure in stamping. This perpendicular lay significantly influences the shear stress in the contact zone. It is most clear in low speeds, less than 27 mm/s in this experimental work, but it cannot be ruled out that it influences friction also at higher speeds. The modeling of these hydrodynamic phenomena was poorly formulated in this work and needs to be improved.

7. Conclusions

- In total 7 parameters are necessary to describe the frictional behavior in its simplest version
- In total 9 to 17 parameters are needed in a more advanced version of the model
- The developed model significantly improved the simulation precision in comparison to Coulomb's friction and provides the user a transparent and controllable tribological system.

Acknowledgements

The research project (Virtual Die Compensation, D.nr. 2015-03480) has been performed within the framework of Metallic materials, a strategic innovation program, run by VINNOVA, the Swedish Energy Agency and the Research Council Formas.

References

[1] S. Zhang. et al.. *A finite element simulation of micro-mechanical frictional behavior in metal forming.* Journal of Materials Processing Technology. 2003. 134 (1 Mar 2003): p. 81 91.
[2] T. Meinders. et al. *Recent developments in finite element simulations of the deep drawing process.* in 5th International Conference on Sheet Metal. 1997. Ulster.
[3] B.H Lee. Y.T Keum. R.H Wagoner. *Modeling of the friction caused by lubrication and surface roughness in sheet metal forming*. Journal of Materials Processing Technology. Volumes 130 131. 20 December 2002. pp. 60 63.
[4] M. Ramezani. Z.M. Ripin. *Effect of friction models on stress distribution of sheet materials during V-bending process*. World Academy of Science. Engineering and Technology. 56. 2009.
[5] T.-C. Hsu. T.-S. Yang. *The computer simulation of tribological influence on strain path and forming limit in punch stretching of sheet metal*. International Journal of Advanced Manufacturing Technology. 2001. 17(6): p. 393 399.
[6] H. Darendeliler. M. Akkok. and C.A. Yucesoy. *Effect of variable friction coefficient on sheet metal drawing*. Tribology International. 2002. 35(2): p. 97 104.
[7] D. Wiklund, B.-G. Rosén, A. Wihlborg, *A friction model evaluated with results from a bending-under-tension test*, Tribology International, Volume 42, Issue 10, 2009, pp. 1448-1452.
[8] J. Hol. M.V. Cid Alfaro. M.B. de Rooij. T. Meinders. *Advanced friction modeling for sheet metal forming*. Wear Volumes 286–287, 15 May 2012, Pages 66–78
[9] J. Hol, V.T. Meinders, H.J.M. Geijselaers, A.H. van den Boogaard, *Multi-scale friction modeling for sheet metal forming: The mixed lubrication regime*, Tribology International 85 (2015) 10–25
[10] National project funded by Swedish Foundation for Strategic Research, SimuPARTS. Dnr: PV08-0041; 2009-2011.
[11] W.C. Emmens. PhD-thesis. University of Twente. Netherlands (1997)
[12] Pullen, J. & Williamson, J.P.B. *On the plastic contact of rough surfaces*, Proc. R. Soc. London, Series A, 1972, 327: 159-173.
[13] H. Christensen. *Stochastic Models for Hydrodynamic Lubrication of Rough Surfaces*,.Proc Instn Mech Engrs. Volumes 184, 1969-70 Pt 1, pp. 1013-1022.
[14] Wilson, W.R.D & Sheu, S. *Real area of contact and boundary friction in metal forming*, International Journal Mechanical Science, 1988, 30(7):475-489.
[15] Sutcliffe, M.P.F., Surface asperity deformation in metal forming processes, International Journal Mechanical Science, 1988, 30(11):847-868.
[16] Challen, J., and Oxley, P., "*An explanation of the different regimes of friction and wear using asperity deformation models*", 1979, Wear 53, pp. 229-243.
[17] Ma, X., Rooij, M., Schipper, D., "*A load dependent friction model for fully plastic contact conditions*", Wear 269, pp. 790-796.
[18] J. O. Hallquist LS-DYNA keyword user's manual. Livermore Software Technology Corporation. 2014.
[19] LS-opt User's manual. Livermore Software Technology Corporation. 2014.